# GPS Derived Strain and Strain Zonation near Charleston, South Carolina

Robert Trenkamp

Department of Geological Sciences, Columbia, SC 29208, USA


Pradeep Talwani

Department of Geological Sciences, Columbia, SC 29208, USA

**Abstract.**   Although the average strain rates within stable continental regions (SCR) are 2-3 orders of magnitude lower than at plate boundaries, pockets of higher strain rates might be expected where large SCR earthquakes have occurred in the past. Recent re-occupation of a 20 station grid near the location of current seismicity (and the inferred location of the 1886 Charleston, South Carolina earthquake) have refined and are consistent with previous shear strain estimates. These refined estimates suggest an average shear strain rate over the study area that is at least an order of magnitude higher than the average intraplate strain rate for the North American Plate east of the Rocky Mountains. Further, subnet (GPS-GPS) strain analysis suggests strain zonation within the study area. The SCR, within which the seismogenic zone is located, has an $\dot\gamma$ of $\sim 10^{-9}$ rad yr$^{-1}$, while the area ($\sim$ 60km x 100 km) immediately surrounding the seismogenic zone has an $\dot\gamma$ of $\sim 5.5$ x $10^{-8} \pm 3.1$ x $10^{-8}$ rad yr$^{-1}$. Within the approximately 20km x 30km region of current, active seismicity, the strain is associated with an $\dot\gamma$ of $\sim 2.1 \times 10^{-7} \pm 1.0$ x $10^{-7}$ rad yr$^{-1}$, two orders of magnitude larger than the background (SCR) strain-rate. The average orientation of the "direction of minimum extension" is consistent with the orientation of measured S$_H$max ($\sim$N60°E).

## 1. Introduction

On August 31, 1886 the largest historical earthquake in the eastern United States occurred near Charleston South Carolina. This Modified Mercalli Intensity X (Bollinger, 1977), M7.3 (Johnston, 1996) earthquake occurring in close proximity to populated areas made it the most destructive U.S. earthquake in the 19th century and the only earthquake east of the Rocky Mountains known to have caused loss of life in the United States.

Paleoseismic evidence of large prehistoric earthquakes along the Atlantic seaboard suggests that large earthquakes ($m_b$=5.8 $\pm$ 0.4) may have been restricted exclusively to South Carolina (Amick and Gelinas, 1991). Paleoliquefaction data suggest the occurrence of seven earthquakes in the past 6,000 years and the more complete data for the past three prehistoric events suggest an average recurrence rate of about 500 years for M=7.0 events near Charleston (Talwani and Schaeffer, 2001).

The tectonic strain rate in stable continental regions is much smaller than at plate boundaries. In the Central and Eastern United States, estimates of strain accumulation range from $10^{-10}$ to $10^{-9}$ per year from Global Positioning System (GPS) data (Dixon et al., 1996) to $10^{-11}$ to $10^{-12}$ per year from an estimate of the seismic strain release (Anderson, 1986) compared to $10^{-7}$ to $10^{-5}$ per year at active

plate boundaries (Kreemer et al., 2002). However Anderson (1986) did note that in areas of large earthquakes in the Eastern United States, i.e. New Madrid Seismic Zone and Charleston, the strain rates were an order of magnitude greater compared to the surrounding regions.

Instrumental seismicity recorded near Charleston between 1974 and 2002 covers an area of about 20km x 30km and has been named the Middleton Place Summerville Seismic Zone (MPSSZ) (Tarr et al., 1981). Recent analysis of the seismicity data suggest that the seismicity occurs by right lateral strike slip faulting along the N-NNE trending Woodstock Fault (WF) which is broken and offset $\sim$5km near Summerville at the NW trending Ashley River Fault (ARF) (Garner 1998). The ARF is associated with reverse fault slip in response to the maximum horizontal stress oriented N60°E. A variety of data suggest that the location of the current seismicity was also the location of the M=7.3, 1886 Charleston Earthquake. In that earthquake over two meters of a railroad track had to be cut to reset the track. With a recurrence rate of 500 years, this 2 m of coseismic shortening suggests an elastic strain accumulation rate of $\sim$4mm per year at the surface.

Various schematic models for Stable Continental Regions (SCR) earthquakes, e.g. the intersection model (Talwani, 1988), stress accumulation near a pluton (Campbell, 1978) and preliminary two-dimensional modeling (Gangopadhyay et al., 2004) all suggest that pockets of stress concentration and therefore increased strain rates could occur in localized volumes although the ultimate source of stress remains enigmatic.

Thus based on the occurrence of the 1886 Charleston earthquake, the accompanying coseismic deformation and
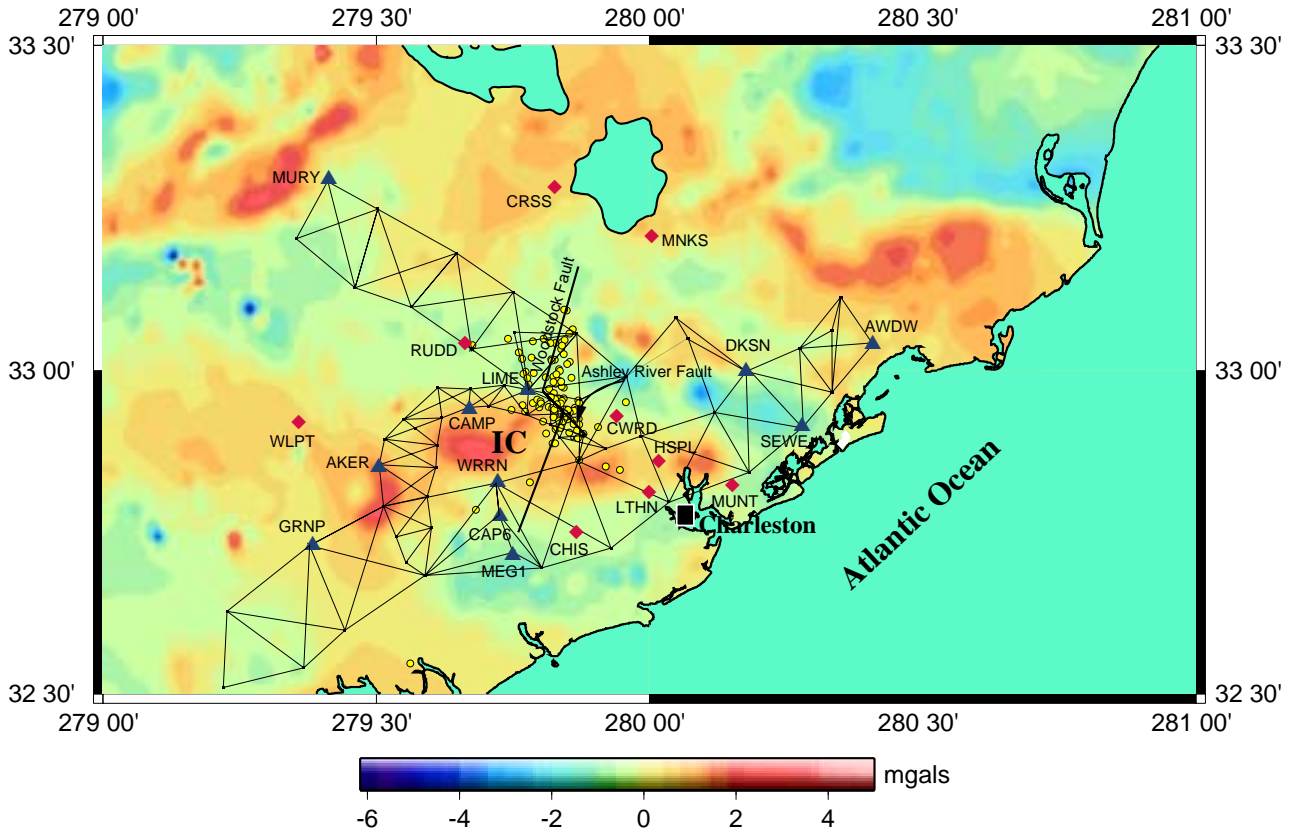
**Figure 1.** Location map of the 20 station GPS grid near the proposed epicenter of the 1886 Charleston earthquake with the triangulation network used in the DYNAP shear strain calculations overlain on residual gravity data (color) (Wildermuth, 2003). Gravity highs are associated with the igneous complex (IC). Fault geometry from Garner (1998). Large blue triangles are the locations of GPS measurements at triangulation sites used in initial triangulation-GPS analysis. Large red diamonds are GPS only sites that were included in the more recent triangulation-GPS analysis.

a record of recurring prehistoric earthquakes, it is expected that the MPSSZ could be a location of stress concentration at which intraplate strain accumulation could be measured using highly sophisticated measurement techniques such as the Global Positioning System.

## 2.  GPS Surveys and Data Analysis

Prescott, et al. (1985), using Franks's method, analyzed some repeated angles in South Carolina which admittedly were not in the immediate vicinity of the 1886 Charleston earthquake. Analysis after splitting the data into two groups, those near the seismic zone and those distant from the seismic zone, yielded values of strain rates that were not significant at even one standard deviation. Previously, attempts to measure strain in the seismogenic zone of the 1886 Charleston earthquake were not undertaken due to the lack of repeat geodetic surveys in the area. The development of GPS as a geophysical tool has given us the ability to obtain precise geodetic measurements with dense spatial sampling.

In December 1993, a reasonably dense grid of 20 stations was selected within a 60 km by 100 km rectangle centered at the MPSSZ (Figure 1) and between December 6, 1993 and January 11, 1994 the first epoch GPS measurements were made. Eleven individual observation sessions averaging 6 hours were scheduled. All sessions were conducted using

6 Trimble 4000 SSE dual frequency receivers with Trimble SST L1/L2 geodetic antennae.

A reoccupation of 17 of the 20 sites in the original grid was performed between February 1 and February 9, 1999. Three sites Ackerman Reset (AKER), Meg (MEG1) and Monks Corner (MNKS) were not observed due to urbanization. The 17 useable stations were observed for at least one 6 hour session and one 3 hour session during times of lowest Geometric Dilution of Precision (GDOP)(Table 1).

A third survey was executed during October and November 2000 (Table 1) during which a 7 station subset consisting of 5 stations near the MPSSZ plus the 2 stations WLPT and SEWE which were continuously occupied during the 1993-1994 campaign. These 7 sites were observed for 2 six hour sessions each.

### 2.1.  Data Processing

All GPS data presented in this study were processed using the JPL/NASA developed GIPSY/OASIS-II (GPS Inferred Positioning System/Orbit Analysis and Simulation Software) software (release 5) (Zumberge et al., 1997). Loosely constrained solutions were obtained using JPL's precise fiducial free orbits and clocks which were then transformed into the International Terrestrial Reference Frame 1996 (ITRF96) through application of daily 7 parameter transformations determined using all IGS tracking stations used in our daily solutions and contained in the ITRF96

**Table 1.** GPS Observations 1993-94, 1998-99, 2000

| dates | AKER | AWDW | CAMP | CAP6 | CHIS | CRSS | CWRD | DKSN | GRNP | HSPL | LIME | LTHN | MEG1 | MNKS | MUNT | MURY | RUDD | SEWE | WLPT | WRRN |
|---|---|---|---|---|---|---|---|---|---|---|---|---|---|---|---|---|---|---|---|---|
| 93dec06 | | | x | | | | | | | x | | x | | x | | | | | x | |
| 93dec07 | | x | | | x | | | | | | | | | | | x | x | x | x | |
| 93dec08 | x | x | | | | | | x | | | | | | | | | x | | x | x |
| 93dec09 | | | | | | | | x | x | | x | | x | | | | | | x | x |
| 93dec14 | | | | | x | x | | x | | | | | | | | x | | | x | x |
| 93dec15 | | | x | x | | | x | | | | | | | | | | x | | x | x |
| 93dec16 | | | | | x | | | | | | | | x | x | | | | x | x | x |
| 94jan10 | | x | | | | | | | | x | | x | | x | | | | | x | x |
| 94jan11 | | x | | x | | | | | | | | x | | | | | | x | x | x |
| 94jan12 | x | | | | | | | x | x | x | | | | | | | | | x | x |
| 94jan13 | | | | x | | | x | | | | x | x | | | | | | | x | x |
| 98dec30 | | | | | | | | | | | | | | | | | | | x | |
| 98dec31 | | | | | | | | | | | | | | | | | | | x | |
| 99feb01 | | x | x | x | x | | | | x | | | x | | | | | x | x | x | x |
| 99feb02 | | | x | | x | | | | x | | | | | | | | x | x | x | |
| 99feb03 | | x | x | x | | | | | | | | | x | | | | x | | x | x |
| 99feb04 | | x | x | x | | x | x | | | x | x | x | | | | | x | | x | x |
| 99feb08 | | x | x | | | x | x | x | | x | | x | | | x | x | | x | | |
| 99feb09 | | x | | | | x | x | | | | | | | | x | x | | x | | |
| 00nov01 | | | | | | | | | | | | | | | | | | | x | |
| 00nov02 | | | | | | | | | | | | | | | | | | | x | |
| 00oct23 | | | x | | | | x | | | x | x | x | | | | | | x | x | |
| 00oct24 | | | x | | | | x | | | x | x | x | | | | | | x | | |
| 00oct31 | | | | | | | | | | | | | | | | | | | x | |

position and velocity model. These are then applied to the daily solutions which transforms them to the desired reference frame (ITRF96).

### 2.2. Site Velocities

Horizontal and vertical velocities (Figure 2, Table 2) were determined using a combination of all 22 daily solutions from the 1993/1994, 1999 and 2000 surveys. A least squares inversion was used to estimate site velocities and position at an arbitrary epoch from the daily ITRF96 coordinates weighted by the full covariance matrix of the coordinates. A scaling factor of 2.184 was applied to the input covariances which is equivalent to scaling the sigmas by 1.5. Variance scaling assumes a Gaussian (normal) error distribution, removal of all human errors (blunders) from the dataset and systematic underestimation of the true errors by GPS software which is generally accepted.

The strain rate signal that we are attempting to measure is presumed to be small. The potential signal should be 4mm or less due to compression of rock at seismogenic depths (3-13kms in the MPSSZ). In order to identify this small surface signal, two approaches were employed: first, shear strain analysis using existing triangulation data combined with the GPS data and second, shear strain and linear strain analysis for GPS sub-networks.

### 2.3. 1920-2000 Shear Strain Analysis

In order to estimate shear strain using data that are not repeatedly measured as is required when using Frank's method (Frank, 1966), the simultaneous reduction method (Bibby, 1982; Drew and Snay, 1989) is used to calculate the maximum horizontal shear strain rate.

The National Geodetic Survey (NGS) supplied available preexisting geodetic observations prior to 1993 (Table 3) from their geodetic database for the area within the 60 km by 100 km rectangle which encompasses the MPSSZ study area (Figure 1). These triangulation data were surveyed between the 1920's and 1990's and in contrast to the GPS data have a precision that is more than an order of magnitude worse, but span a much longer time. The datasets are combined and DYNAP is used to not only generate the least squares estimates for the positional coordinates of the stations but also, simultaneously, for parameters that characterize crustal deformation rates. A spatially uniform and constant deformation rate during the time interval is assumed (for details see Drew and Snay, 1989).

**Table 2.** East, North and Vertical Vectors Relative to ITRF96

| site | longitude deg | latitude deg | East mm/yr | 1$\sigma$ | North mm/yr | 1$\sigma$ | Vert mm/yr | 1$\sigma$ |
|---|---|---|---|---|---|---|---|---|
| WRRN | -80.28 | 32.82 | -11.52 | 2.25 | 1.31 | 1.65 | 7.64 | 4.23 |
| LTHN | -80.00 | 32.81 | -13.03 | 1.53 | 0.84 | 1.39 | -0.29 | 3.17 |
| SEWE | -79.72 | 32.91 | -12.20 | 1.45 | 1.75 | 1.32 | 0.17 | 2.65 |
| CAMP | -80.33 | 32.94 | -10.14 | 2.02 | -0.94 | 1.56 | 0.91 | 4.20 |
| CAP6 | -80.27 | 32.78 | -13.32 | 1.56 | 1.57 | 1.41 | -0.17 | 3.20 |
| RUDD | -80.32 | 33.03 | -10.66 | 1.87 | 0.48 | 1.54 | -0.42 | 3.92 |
| CHIS | -80.13 | 32.75 | -12.32 | 2.25 | 1.03 | 1.58 | 2.82 | 4.10 |
| MUNT | -79.85 | 32.83 | -13.64 | 1.98 | 2.38 | 1.58 | -1.78 | 4.29 |
| CRSS | -80.17 | 33.28 | -12.44 | 1.70 | 0.31 | 1.46 | -0.82 | 3.79 |
| CWRD | -80.06 | 32.93 | -13.08 | 1.85 | 1.21 | 1.53 | -2.77 | 3.66 |
| DKSN | -79.82 | 33.00 | -13.97 | 1.76 | 2.34 | 1.45 | -8.65 | 3.56 |
| MURY | -80.59 | 33.29 | -11.08 | 2.02 | 0.67 | 1.63 | 0.84 | 4.46 |
| LIME | -80.22 | 32.97 | -13.61 | 1.52 | 0.87 | 1.37 | -4.22 | 2.98 |
| GRNP | -80.62 | 32.73 | -11.69 | 1.93 | 1.41 | 1.56 | 0.93 | 4.14 |
| WLPT | -80.64 | 32.92 | -13.27 | 1.39 | 0.80 | 1.29 | -1.12 | 2.45 |
| HSPL | -79.98 | 32.86 | -12.77 | 1.54 | 0.95 | 1.38 | -1.68 | 3.05 |
| AWDW | -79.59 | 33.04 | -10.56 | 2.14 | 4.53 | 1.68 | 0.93 | 4.80 |
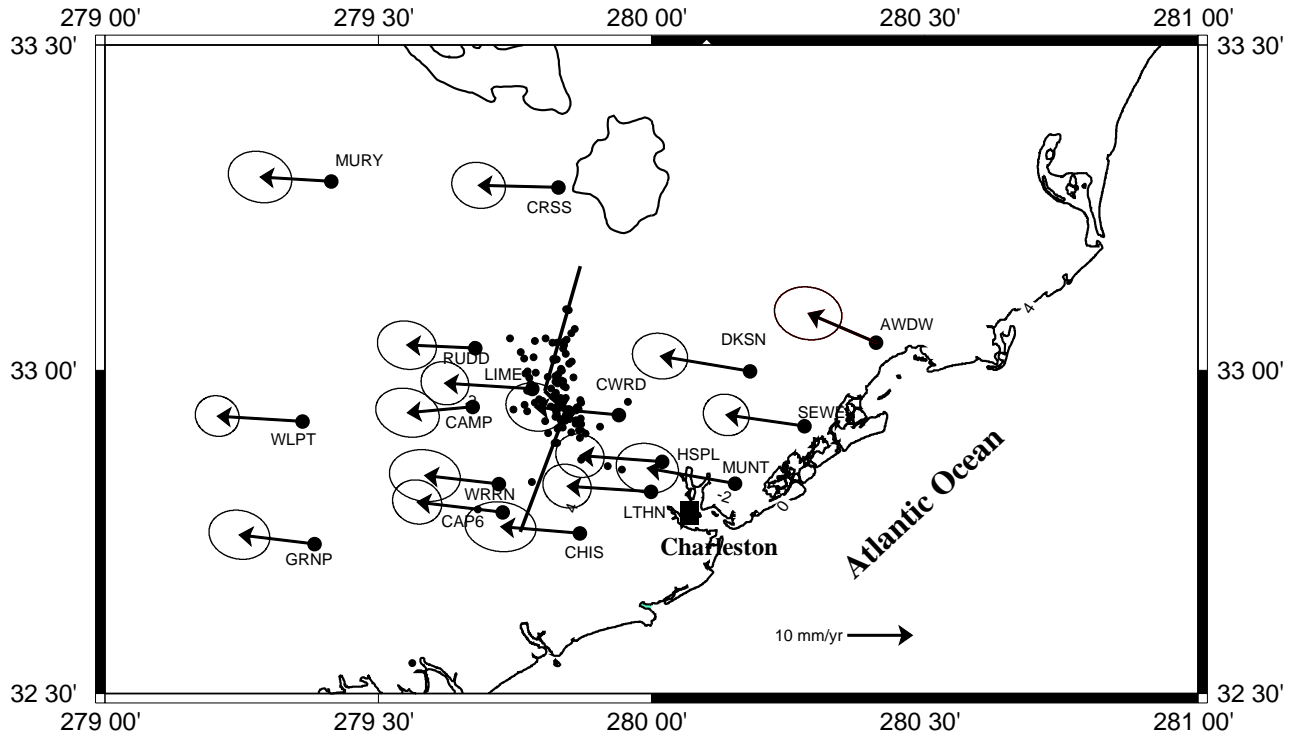
**Figure 2.** Horizontal velocity vectors with $2\sigma$ errors in mm/yr relative to the ITRF96 reference frame. Small black dots concentrated around the fault intersection indicate the location of recent microseismicity.

Initial solution of the shear strain analysis performed after the 1993/1994 surveys resulted in a measured strain rate of $0.041 \pm 0.017$ $\mu$rad yr$^{-1}$ at $66° \pm 11°$ (Table 4)(Trenkamp, 1996; Talwani et al., 1997) which, although not significant at 95% confidence, is significant at 90% confidence and implies a strain rate in the MPSSZ approximately two orders of magnitude greater than the rate for the North American Plate ($10^{-10}$ to $10^{-9}$) east of the Rocky Mountains (Dixon et al., 1996; Snay and Strange, 1997).

Since the initial 20 station network consisted of several sites that were not coincident with sites used for the triangulation surveys, the initial strain rate calculations did not include these GPS specific sites (Figure 1). Also, anomalously large residual motions at station Awendaw 2 ( AWDW) were measured during the GPS resurvey. Therefore, station AWDW's GPS measured values were removed from all strain rate analysis. The addition of the 1999-2000 GPS resurvey data resulted in a refined shear strain rate of 0.022 $\pm 0.01$ $\mu$rad yr$^{-1}$ @ $52° \pm 11°$ (Table 4). Although this more recent and more robust analysis of shear strain rate did not produce a strain rate significant at the 95% confidence level, it did reaffirm at the 90% confidence level a measured shear

strain rate approximately two orders of magnitude greater than the average strain rate measured in the North American Plate east of the Rocky Mountains.

### 2.4. 1993-2000 Shear Strain Analysis

In order to refine the understanding of the strain distribution within the study area, a regional sub-network was developed containing a subset of the 16 useable GPS vectors (Figure 3 excluding AWDW). Relative positions among closely spaced GPS sites are well determined due to cancellation of common mode errors. The ITRF96 daily solutions of the sub-network were input as quasi observations into the *Quasi Observations Combination Analysis* (QOCA) software developed at the JPL (Dong et al., 1998) to solve for the velocity gradient tensor components. Results of the sub-network analysis are summarized in Table 5 as the eigenvalue parameterization ($\dot{\epsilon}_1, \dot{\epsilon}_2, \theta, \dot{\omega}$) along with the $\dot{\gamma}$ evaluation for ready comparison to the previous shear strain estimates. These GPS data are fully three dimensional and are sensitive to areal dilatation which is only poorly determined with DYNAP although our particular triangulation dataset

**Table 3.** NGS supplied Geodetic Observations and GPS observations used in study

| Interval | Directions | Distances | Azimuths | GPS Obs. |
|---|---|---|---|---|
| 20-29 | 533 | 10 | 1 | 0 |
| 30-39 | 1370 | 12 | 2 | 0 |
| 40-49 | 116 | 0 | 0 | 0 |
| 50-59 | 26 | 0 | 2 | 0 |
| 60-69 | 373 | 217 | 4 | 0 |
| 70-79 | 0 | 11 | 1 | 0 |
| 80-89 | 618 | 162 | 8 | 0 |
| 90-99 | 6 | 6 | 1 | 117 |
| 2000 | 0 | 0 | 0 | 16 |

**Table 4.** NGS + GPS estimated shear strain rates

| Dataset NGS + GPS | $\dot{\gamma}_1 = \epsilon_{EE} - \epsilon_{NN}$ $\mu$rad yr$^{-1}$ | $\dot{\gamma}_2 = \epsilon_{EN} - \epsilon_{NE}$ $\mu$rad yr$^{-1}$ | $\dot{\gamma} = (\dot{\gamma}_1 + \dot{\gamma}_2)^{\frac{1}{2}}$ $\mu$rad yr$^{-1}$ | $\theta = .5\tan^{-1}(\dot{\gamma}_2)/\dot{\gamma}_1)^{\frac{1}{2}}$ degrees |
|---|---|---|---|---|
| NGS + 93-94 | -0.027 ± 0.016 | -0.031 ± 0.017 | 0.041 ± 0.017 | 66° ± 11° |
| NGS + 93-00 | -0.005 ± 0.009 | -0.021 ± 0.010 | 0.022 ± 0.010 | 52° ± 11° |

contained 19 azimuths distributed throughout the data years (Table 3). A model(Talwani and Gagopadhyay, 2000) which predicts the strain distribution maintains that the higher strains should be concentrated near the fault intersections and intrusive bodies that may influence the location of the microseismicity (Figure 1). An approximate order of magnitude increase in the shear strain rate estimate for the six station inner regional sub-network is noted when compared to the full network shear strain rate estimate.

The six stations that comprise the inner regional sub-network span the area of the Ashley River - Woodstock Fault (ARWF) intersection and straddle the igneous complex (IC) around which the local microseismicity clusters (Figure 3). Using the six stations of the inner regional sub-network, four subnets were developed as Delaunay triangles (Feigl et al., 1993) and processed to calculate the shear strains within each. Two of the four subnets accumulated significant shear strain between 1994 and 2000 at the formal 95% confidence level. The significantly straining subnets are subnet 1 (CAMP LIME LTHN) which is composed of stations that span the area defined by the left step of the intersection of the ARWF and the IC and subnet 4 (CAMP RUDD LIME) which straddles the northwest edge of the IC. subnet 1 has a principal shortening direction (68° ± 6°) that is

approximately along the preferred orientation (N60°E) (Talwani, 1982; Zoback and Zoback, 1991) for applied stress in the eastern U.S. whereas subnet 4 has a principal shortening direction that is rotated to an east-west orientation (90° ± 10°).

The maximum shear strain rates for both subnet 1 and subnet 4 ($\sim$.5 ± .1 $\mu$rad yr$^{-1}$) are 25 times greater than that expected from the maximum shear strain rate determined initially (.022 ± .01 $\mu$rad yr$^{-1}$) using the full triangulation-GPS dataset. Common to both strained subnets are the stations CAMP and LIME. Vector residuals relative to station WLPT suggest that CAMP has the anomalously large residual vector magnitude which may explain the high strain rates found in the subnets (Figure 3). Subnet 1 also has a significant rotation rate (-2.6 x 10$^{-7}$ yr$^{-1}$) at 2$\sigma$ whereas all other subnet rotations are not significant at 2$\sigma$ although the rotation rate at subnet 4 is also elevated (Table 5)

### 2.5. Linear strain rates

One of the simplest methods to investigate strain accumulation and the specific sites that are responsible for it is to estimate linear strain accumulation rates from GPS baseline vectors. Due to the constant GPS orbital distance from the center of mass of the Earth, length scaling errors
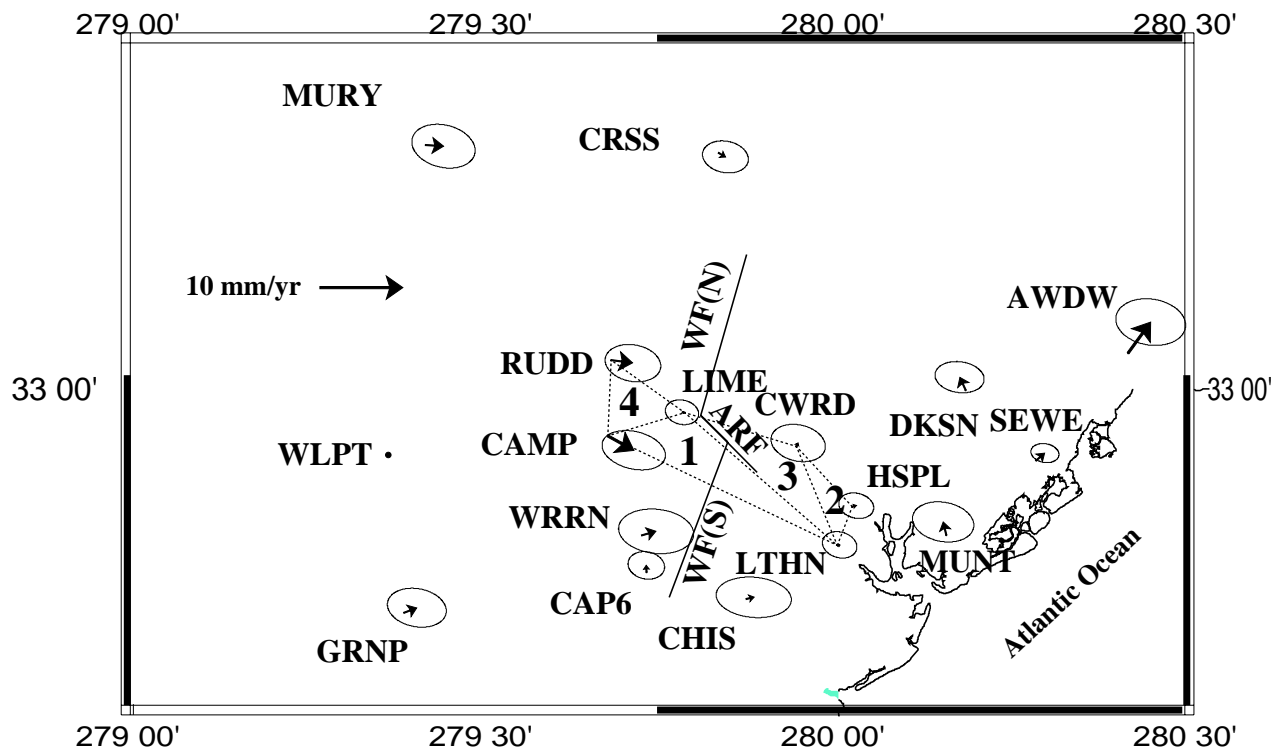


**Figure 3.** Inner regional six station sub-network over which the strain rate was estimated. Also shown are the Delaunay triangles (subnets labeled 1-4) over which the shear strain was also estimated. WF(N) and WF(S) are the north and south branches of the Woodstock fault which are offset by the northwest trending Ashley River Fault (ARF). GPS vectors with 95% confidence ellipses are shown relative to WLPT which is considered outside the straining zone and equivalent to North America Plate motion.
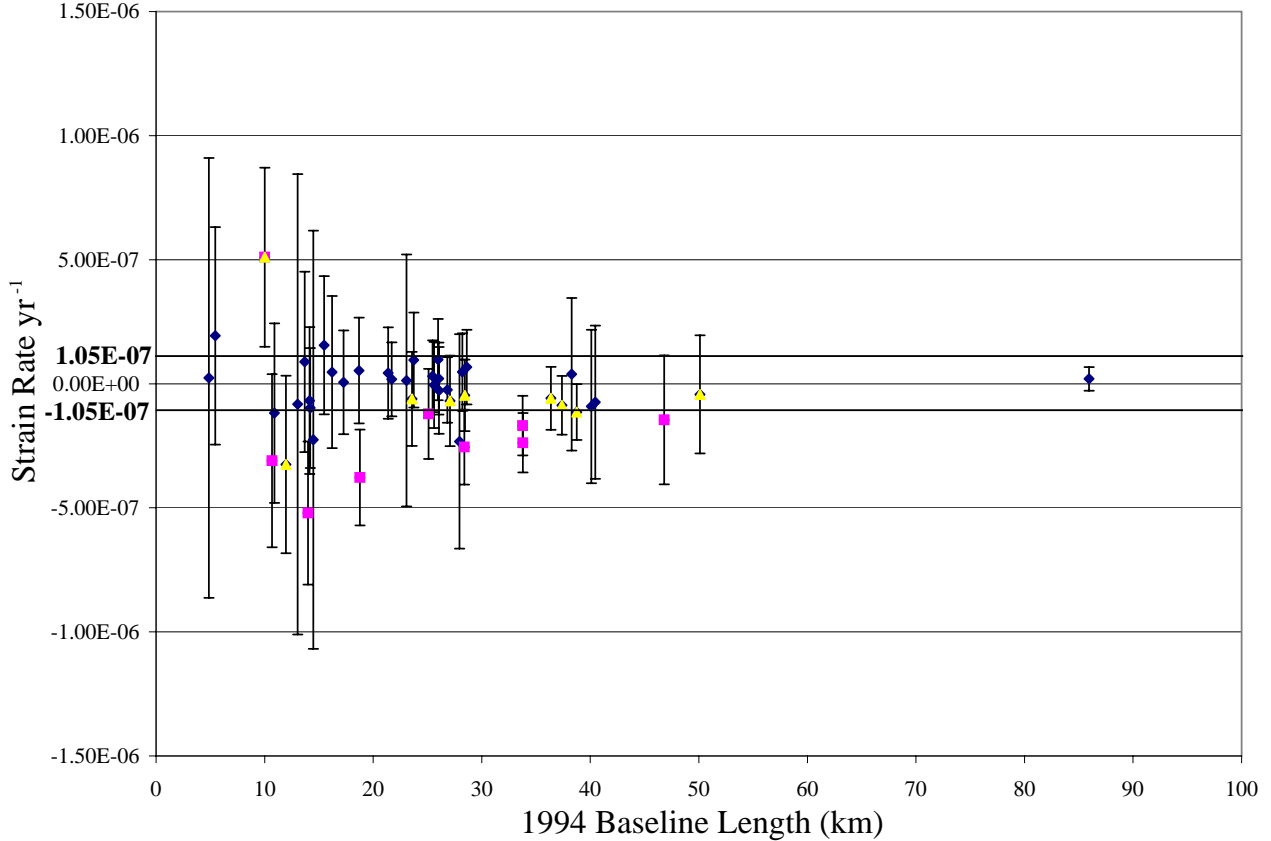
**Figure 4.** Linear baseline vectors strain plotted relative to their length from the nine stations within and around the regional sub-network with the upper bound 1.05E-07 plotted as thick black lines. The squares are those baselines that include station CAMP and the triangles are those baselines that include station RUDD

between successive GPS measurement epochs are negligible. Therefore it is possible to estimate linear strain rates from our repeated campaign baseline vectors. Since there is an apparent order of magnitude increase in the shear strain rate within the inner regional sub-network, the baseline vectors determined by these six stations combined with three other nearby stations (CHIS, CAP6, MUNT) (Figure 3) were used to compose the subset of baseline vectors to investigate what may be causing the ultra high strains that are measured.

In order to obtain scalar linear strain rates for an individual baseline vector $\mathbf{V}$, a simple calculation is performed (following Weber et al., 1998)

$$\dot{e} = [(V_i - V_{1994})/V_{1994}]/dt$$

where $V_i$ is the more recent baseline vector length (1999 or 2000) and dt is the time between the observations. It is assumed that there are no correlations between baselines lengths and that there are no unmodeled errors. The actual scaled errors as reported for the individual baseline lengths were used and are believed to be fairly conservative as scaled. The linear strain rates with their $1\sigma$ errors are plotted in Figure 4 relative to their length for all the possible baselines within and around the inner regional network. These data constrain the maximum possible average linear strain rates for the area ($\dot{e}$) to be less than $9.1 \times 10^{-7}$ strain $\mathrm{yr}^{-1}$. The actual maximum regional strain rate must be smaller than this for two reasons. First, this rate is approaching the long term strain rates that are measured within 100 km of plate boundary fault zones ($1 \times 10^{-5}$ to $1 \times 10^{-6}$ $\mathrm{yr}^{-1}$) (Bilham et

al,.1989) and is not sustainable for the 500-600 year repeat times that have been determined for the area (Talwani and Schaeffer, 2001); second, a large number of the observations (89%) include zero as a possible strain rate at $1\sigma$ suggesting that the actual strain rate could and should be much lower than this maximum.

Comparison of maximum shear strain rates ($\dot{\gamma}$) derived from the combination of triangulation and GPS data ($0.22 \times 10^{-7} \pm 0.10 \times 10^{-7}$ rads $\mathrm{yr}^{-1}$) (Table 4) and the maximum shear strain rate derived from GPS for the inner regional sub-network ($2.1 \times 10^{-7} \pm 1.0 \times 10^{-7}$ rad $\mathrm{yr}^{-1}$) (Table 5) suggest that the network may not be accumulating strain homogeneously which is one of the core assumptions of the DYNAP software version used in this study but that, although all the area within the 60 x 100 km rectangle may have a higher average strain rate than the general rigid plate interiors ($10^{-9}$ strain $\mathrm{yr}^{-1}$), there may be pockets of even higher strain within that area.

Snay et al. (1994) showed that linear strain ($\dot{\epsilon}$) and shear strain ($\dot{\gamma}$) are not directly comparable but are related as

$$\dot{\gamma} = \dot{\epsilon}_1 - \dot{\epsilon}_2$$

from which follows

$$\dot{\gamma} \leq 2\dot{\epsilon}$$

for shear strain rates expressed in *radians per year* and linear strain rates expressed in units of *strain per year* (*see also* Weber et al., 1998).

Therefore the highest shear strain rates reported for the total network ($\dot{\gamma} = 0.22 \times 10^{-7}$ rad $\mathrm{yr}^{-1}$) implies an upper bound on the total regional linear strain rates of $\dot{\epsilon} \leq$
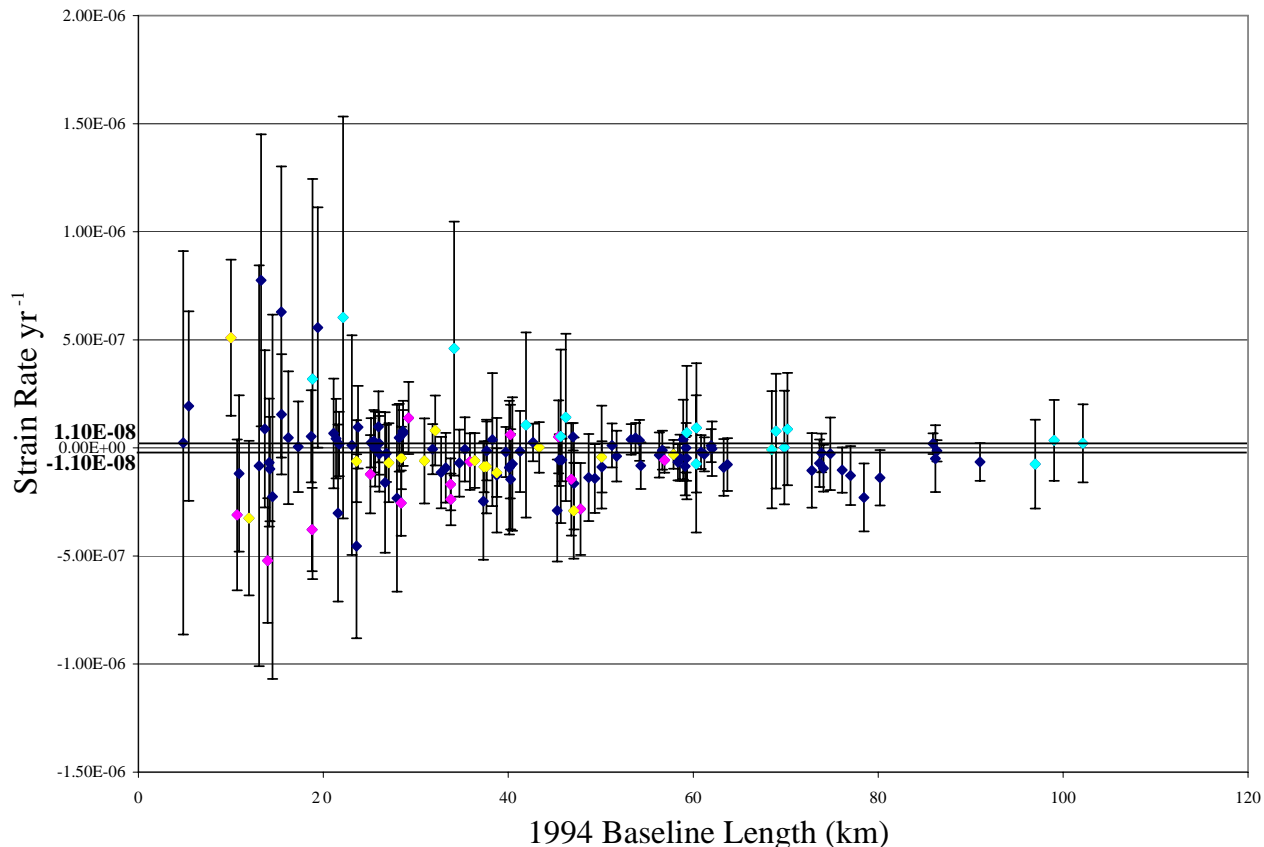
**Figure 5.** Linear baseline vectors plotted relative to their length from all stations including Awendaw 2 (AWDW) with the upper bound 1.10E-08 plotted. Blue diamonds are baselines that include station AWDW, the yellow diamonds are those baselines that include station RUDD and the purple diamonds are those baslines that include station CAMP.

0.11 x $10^{-7}$ strain $yr^{-1}$. Only 13 of the 136 baseline vectors fit this criteria whereas most imply higher rates (Figure 5). The shear strain rate reported for the inner regional sub-network ($\dot{\gamma} = 2.1$ x $10^{-7}$ rad $yr^{-1}$) implies an upper bound on the total inner regional linear strain rates of $\dot{\epsilon} \leq 1.05$ x $10^{-7}$ strain $yr^{-1}$. Only 14 of the 46 (30%) have allowable strain rates higher than this whereas most imply lower rates. Interestingly, the one station that is involved in 9 of the 14 (64%) baselines that have allowable strain rates higher than the upper bound is station CAMP (Figure 4).

In order to judge the influence of individual stations on the estimated strain field which was measured over the inner regional sub-network, different combinations of stations were evaluated to determine how each station was contributing to such high measured values. The removal of CAMP and RUDD individually resulted in a measured strain rate drop of approximately 25% and the linear strain rates ($\dot{\epsilon_1},\dot{\epsilon_2}$) were each reduced by similar amounts (Table 5). When both RUDD and CAMP were removed, the shear strain rate dropped 68% and the linear strain rates ($\dot{\epsilon_1},\dot{\epsilon_2}$) both turned extensional (Table 5). The removal of CWRD reduced the inner regional sub-network to the three stations LIME HSPL and LTHN which after analysis increased the measured shear strain rate marginally and returned a compressional component to $\dot{\epsilon_2}$. Along with the changes of rate, the angle of minimum extension ($\theta$) also changed rather drastically with the changing geometries (Table 5). No combination of stations in the inner regional subnetwork gave an estimate of

shear strain rate smaller than 0.46 x $10^{-7}$ rad $yr^{-1}$ or twice the rate estimate for the triangulation-GPS shear strain rate for the whole network (0.22 x $10^{-7}$ rad $yr^{-1}$) and the linear strain rate for the direction of maximum contraction($\dot{\epsilon_2}$) for the LIME HSPL LTHN subnet is at least 1.5 times greater than $\dot{\epsilon_2}$ for the 7 station outer sub-network (Table 5).

Snay (1986) showed that small changes in network geometry -inclusion or exclusion of a few measurements- can change results significantly when analyzing triangulation data for estimating strain accumulation rates in intraplate settings. Aside from possible human error, GPS has its own suite of potential problems which must be continuously considered when interpreting GPS data and any estimates derived from them. Primarily error estimation is always a problem and conservative is the preferred manner of error estimation and it is always important to remember that GPS measures all motions related to the monument not just the motion that is sought. Although the shear strain determined for the inner regional sub-network is not extreme as averaged over the entire area , it is obvious that the shear strain rates measured at the two subnets (1 & 4) (Table 5) are not sustainable in the intraplate setting for long periods of time and are probably directly related to the vector at CAMP. These assumptions are supported by the measured linear strain rates that placed every linear strain value measured with CAMP outside the upper bound for the total inner regional linear strain rates. Such large strain rates must be the result of another signal overprinting the horizontal tectonic

signal which is then also being added to the horizontal strain estimates. Possible scenarios include monument instability related to recent drought conditions affecting monuments in alluvium and possible vertical tectonic motions which may or may not be part of an emerging strain signal. Table 2 and Figure 2 shows that at least 2 stations that have large vertical motions are in the area of the inner regional sub-network. The contours of vertical motion suggest that CAMP RUDD and CWRD are all possibly affected by vertical signal overprinting that is enhancing or subtracting from their true three dimensional tectonic signal.

## 3. Summary and Conclusions

Analysis of the geodetic data available for the inferred epicentral area of the 1886 Charleston Earthquake demonstrate the challenge involved in attempting to estimate strain accumulation rates in a stable continental region overlain by a thick sedimentary package. Most of the sites measured using the GPS were the less stable older monuments that were part of the previous triangulation networks, especially near the seismogenic zone. These older sites were initially used in order to get a rapid first estimation using the combined triangulation-GPS dataset and because they were the only sites available in the area. Very few sites near the fault intersection and seismogenic structures were established expressly for GPS measurements and none were established for the express purpose of measuring strain in areas where the noise to signal ratio is high.

With these considerations in mind, the strain orientation is generally consistent with measured $S_H$max ($\sim$N60°E) (Talwani, 1982; Zoback and Zoback, 1991) and the data reported here do suggest that a measureable strain signal is emerging from these initial observations. Most of the reported strain measurements are significant at $1\sigma$ and are consistent with the initial measurements and expected values in both magnitude and azimuth. These observations indicate strain zonation, with a small area ($\sim$20km x 30km) of high strain rate accumulation ($\sim$2.1x10$^{-7}$ ± 1.0x10$^{-7}$ rad yr$^{-1}$) surrounded by a broader ($\sim$ 60km x 100km) area of elevated strain rate accumulation ($\sim$0.22x10$^{-7}$ ± 0.10x10$^{-7}$ rad yr$^{-1}$) lying in a SCR characterized by a strain rate of $\sim$10$^{-9}$ rad yr$^{-1}$. The region of largest measured strains coincide with locations of current seismicity near the seismogenic portions of the Ashley River fault where it intersects and offsets the Woodstock fault. The observed strains in the MPSSZ are also consistent with the schematic model

for intraplate earthquakes which predicts pockets of elevated stress (and strains) near fault intersections (Talwani and Gangopadhyay, 2000). These field observations are also consistent with the results of two-dimensional mechanical modeling of the MPSSZ, the results of which suggest elevated strains between the intersection of the Ashley River fault with the southern and northern legs of the Woodstock fault (Gangopadhyay and Talwani, 2004)

The exceptionally large strain rates associated with measured vectors at both CAMP and RUDD are probably the result of some non-tectonic overprinting. These motions require closer analysis and quantification which can be accomplished by investigation of other available data (e.g. well pumping rates, INSAR positional data) within the area and densifying the area within the seismogenic zone with more stable GPS sites suitable for the alluvium in which they are monumented. These densified and more stable monuments will enable the clarification of the strain variance which the existing measurements suggest are occurring at and near the fault/igneous complex interplay.

## References

Amick, D., and R. Gelinas, The search for evidence of large prehistoric earthquakes along the Atlantic seaboard, *Science, 251*, 655-658, 1991.

Anderson, J.G., Seismic strain rates in the central and Eastern United States, *Bull. Seis. Soc. Am., 76*, 273-290, 1986.

Bibby, H.M., Unbiased estimate of strain from triangulation data using the method of simultaneous reduction, *Tectonophysics, 82*, 161-174, 1982.

Bilham, R., R.S. Yeats, and S. Zerbini, Space geodesy and the global forecast of earthquakes, *Eos, Trans. AGU, 70*, 65, 73, 1989.

Bollinger, G.A., Studies related to the Charleston, South Carolina, earthquake of 1886 - A preliminary report, in *Reinterpretation of the intensity data for the 1886 Charleston, South Carolina, earthquake*, 17-32, 1977.

**Table 5.** Inner Sub-network and Subnets - Outer Sub-network strain estimates. Subnets are composed of Delaunay Triangles as (1) CAMP-LIME-LTHN (2) CWRD-LTHN-HSPL (3) LIME-CWRD-LTHN (4) CAMP-RUDD-LIME

| Subnet | $\dot{\epsilon_1}$ $10^{-8}$ strain yr$^{-1}$ | $\dot{\epsilon_2}$ $10^{-8}$ strain yr$^{-1}$ | $\dot{\omega}$ $10^{-8}$ strain yr$^{-1}$ | $\theta$ deg | $\dot{\gamma}$ $10^{-8}$ rad yr$^{-1}$ |
|---|---|---|---|---|---|
| Inner | .860 ± .700 | -12.4 ± 7.24 | -10.2 ± 5.94 | 80 ± 13 | 21.0 ± 10.0 |
| **1** | **15.3 ± 7.90** | **-36.7 ± 11.8** | **-25.8 ± 7.83** | **68 ± 6** | **52.0 ± 14.2** |
| 2 | 5.37 ± .107 | -12.7 ± 27.8 | -.876 ± 13.7 | 77 ± 39 | 18.1 ± 29.8 |
| 3 | 19.5 ± 17.6 | 3.88 ± 6.58 | -1.53 ± 10.7 | -37 ± 34 | 15.6 ± 18.8 |
| **4** | **8.26 ± 9.54** | **-40.1 ± 10.9** | **-7.65 ± 8.92** | **90 ± 10** | **48.4 ± 14.5** |
| No CAMP | 6.04 ± 14.7 | -8.83 ± 10.8 | -4.64 ± 10.0 | 93 ± 34 | 14.9 ± 18.2 |
| No RUDD | 5.47 ± 8.76 | -8.61 ± 4.66 | 3.32 ± 6.45 | 120 ± 33 | 14.1 ± 9.92 |
| No CAMP-RUDD | 8.86 ± 15.0 | 4.25 ± 3.59 | -4.05 ± 10.2 | 123 ± 130 | 4.61 ± 15.4 |
| No CAMP-RUDD-CWRD | 4.85 ± 8.01 | -1.98 ± 19.2 | -6.11 ± 12.0 | 53 ± 86 | 6.83 ± 20.8 |
| Outer | 4.20 ± 2.02 | -1.29 ± 2.39 | -.040 ± .956 | 48 ± 16 | 5.49 ± 3.13 |

Campbell, D.L., Investigation of the concentration mechanism for intraplate earthquakes, *Geophys. Res. Lett., 5*, 477-499, 1978.

Dixon, T.H., A. Mao, and S. Stein, How rigid is the stable interior of the North American Plate?, *Geophys. Res. Lett., 23*, 3035-3038, 1996.

Dong, D., T.A. Herring, and R.W. King, Estimating regional deformation from a combination of space and terrestrial geodetic data, *J. of Geodesy, 72*, 200-214, 1998.

Drew, A.R., and R.A. Snay, DYNAP; software for estimating crustal deformation from geodetic data, *Tectonophysics, 162*, 331-343, 1989.

Feigl, K.L., D.C. Agnew, Y. Bock, D. Dong, A. Donnellan, B.H. Hager T.A. Herring, D.D. Jackson, T.H.Jordan, R.W. King, S. Larsen, K.M. Larson, M.H. Murray, Z. Shen, and F.H. Webb, Space geodetic measurement of crustal deformation in Central and Southern California, 1984-1992, *J. Geophys. Res., B, Solid Earth and Planets, 98*, 21677-21712, 1992.

Frank, F.C., Deduction of earth strains from survey data, *Bull. Seis. Soc. Am., 56*, 35-42, 1966.

Gangopadhyay, A., J. Dickerson and P. Talwani, A Two - dimensional Numerical Model for current seismicity in the New Madrid seismic zone,*Seis. Res. Lett.*. 75, 406-418, 2004.

Gangopadhyay, A. and P. Talwani, Fault interactions and intraplate seismicity in Charleston, South Carolina; insights from a 2-D numerical model, *Current Science, in press*, 2004.

Garner, J., Re-evaluation of the Seismotectonics of the Charleston, South Carolina Area, *Masters thesis*, 250 pp., University of South Carolina, Columbia, 1998.

Johnston, A.C., Seismic movement aassessment of earthquakes in stable continental regions; III, New Madrid 1811-1812, Charleston 1886 and Lisbon 1755, *Geophys. J. Intl.*, 126, 314-344, 1996.

Kreemer, C., W.E. Holt, and A.J. Haines, The Global Moment Rate Distribution within Plate Boundary Zones, in *Plate Boundary Zones, AGU Monograph Series* 173-190, 2002.

Prescott, W.H., S.W. Krueger, and M.D. Zoback, Geodetic constraints on strain rates in the vicinity of the 1886 Charleston, South Carolina, earthquake, in *Proceedings of the first international symposium on precise positioning with GPS, Rockville, Maryland, U.S. Dept. of Commerce, NOAA, NOS*, Vol. II, 887-896, 1985.

Snay, R.A., Horizontal deformation in New York and Connecticut; examining contradictory results from the geodetic evidence, *J. Geophys. Res., B, Solid Earth and Planets, 91*, 12,695-12,702, 1986.

Snay, R.A., J.F. Ni, and H.C. Neugebauer, Geodetically Derived Strain Across the New Madrid Seismic Zone, F1- F6 pp., *U.S.G.S. Prof. Paper 1538*, 1994.

Snay, R.A., and W.E. Strang, Horizontal Velocities in the central and eastern United States from GPS surveys during the 1987-1996 interval, pp. 27, NUREG/CR-6586 *U.S. Nuclear Regulatory Commission*, Washington, DC 20555, 1997.

Talwani, P., Internally cosistent pattern of seismicity near Charleston, South Carolina, *Geology*, 10, 654-658, 1982.

Talwani, P., The Intersection Model for Intraplate Earthquakes, *Seism. Res. Lett., 59*, 305- 310, 1988.

Talwani, P., J.N. Kellogg, and R. Trenkamp, Validation of Tectonic Models for an Intraplate Seismic Zone, Charleston, South Carolina, with GPS Geodetic Data, pp. 41,NUREG/CR-6529 *U.S. Nuclear Regulatory Commission*, Columbia, 1997.

Talwani, P. and A. Gangopadhyay, Schematic model for intraplate earthquakes, *EOS, Trans. AGU.*, 81, F918, 2000.

Talwani, P., and W.T. Schaeffer, Recurrence rates of large earthquakes in the South Carolina coastal plain based on paleoliquefaction data, *J. Geophys. Res., B, Solid Earth and Planets, 106*, 6621-6642, 2001.

Tarr, A.C., P. Talwani, S. Rhea, D. Carver and D. Amick, Results of rescent South Carolina seismological studies, *Bull. Seis. Soc. Am.*, 71,1883-1902, 1981.

Trenkamp, R.A., Geodetic Strain Analysis in the Summerville South Carolina Area, *Masters thesis*, 96 pp., University of South Carolina, Columbia, 1996.

Weber, J., S. Stein, and J. Engeln, Estimation of intraplate strain accumulation in the New Madrid seismic zone from repeat GPS surveys, *Tectonics, 17*, 250-266, 1998.

Wessel,P. and W.H.T. Smith, New version of the generic mapping tools released. *EOS Trans. AGU.*, 76, 329.

Zoback, M.D., and M.L. Zoback, Tectonic Stress Field of North America and Relative Plate Motions, in Neotectonics of North America: Boulder, Colorado, *Geological Society of America, Decade Map, vol. 1, edited by D.B. Slemmons, E.R. Engdahl, M.D. Zoback and D.D. Blackwell,* pp. 339-366, 1991.

Zumberge, J.F., M.B. Heflin, D.C. Jefferson, M.M. Watkins, and F.H. Webb, Precise point positioning for the efficient and robust analysis of GPS data from large networks, *J. Geophys. Res., B, Solid Earth and Planets, 102*, 5005-5017, 1997.

Robert Trenkamp, Pradeep Talwani, Department of Geological Sciences, University of South Carolina, Columbia, SC 29208, USA. (trenkamp@geol.sc.edu) (pradeep@sc.edu)